Vol 16 No 1, January 2007
1009-1963/2007/16(01)/0032-06

Chinese Physics

© 2007 Chin. Phys. Soc.
and IOP Publishing Ltd

Parallel numerical simulations for quantized vortices in Bose–Einstein condensates*

Huang Zhao-Hui(黄朝晖)[a)†] and Wang De-Sheng(王德生)[b)]

[a)] *State Key Laboratory of Space Weather, Center for Space Science and Applied Research, Chinese Academy of Sciences, Beijing* 100080, *China*

[b)] *Department of Civil Engineering, University of Wales Swansea, Singleton, Swansea, UK*

(Received 13 March 2006; revised manuscript received 14 August 2006)

We employ the parallel computing technology to study numerically the three-dimensional structure of quantized vortices of Bose–Einstein condensates. For anisotropic cases, the bending process of vortices is described in detail by the decrease of Gross–Pitaevskii energy. A completely straight vortex and the steady and symmetrical multiple-vortex configurations are obtained. We analyse the effect of initial conditions and angular velocity on the number and shape of vortices.

Keywords: 3D numerical simulations, quantized vortices, Bose–Einstein condensates, parallel computing

PACC: 0365, 0530, 0570

1. Introduction

Recently, the Ecole Normale Superieure (ENS) group[1,2] has studied a single vortex line and observed planar U-shaped vortices but also S-shaped ones. Du *et al* theoretically and numerically gave critical velocities, energy diagrams and vortex configurations in rotating Bose–Einstein condensates (BECs),[3–6] based on which we have conducted a series of three-dimensional (3D) numerical simulations and obtained a single completely straight vortex and multiple bending vortices. Liu *et al* also investigated BECs in depth.[7–9] Lu discussed exact solutions for nonlinear Schrödinger equation in phase space.[10] Xu *et al* gave the single vortex solution in Ref.[11].

2. Model and solution

We consider the case of a condensate being placed in a rotating frame with an angular velocity $\boldsymbol{\Omega} = \Omega \boldsymbol{e}_z$, and the wave function ϕ minimizes the Gross–Pitaevskii energy $E_{3\mathrm{D}}(\phi) = \int h^2/(2m)|\mathrm{grad}(\phi)|^2 + m/2\sum_{\alpha}\omega_{\alpha}^2 r_{\alpha}^2|\phi|^2 + N/2g_{3\mathrm{D}}|\phi|^4 - h\boldsymbol{\Omega}\cdot(\mathrm{i}\phi, \mathrm{grad}\,\phi \times \boldsymbol{x})$ under the constraint $\int|\phi|^2 = 1$. Here, for any complex quantities u, v and their complex conjugates u', v', we have $(u, v) = (uv' + u'v)/2$. By introducing the characteristic length $d = (h/m\omega_x)^{1/2}$and rescaling the distance $R = d/\sqrt{\varepsilon}$ where $\varepsilon^2 = h^2/(2N_g m)$, defining the new variable $u(\boldsymbol{r}) = R\phi(\boldsymbol{x})$ where $\boldsymbol{x} = R\boldsymbol{r}$, and setting $\boldsymbol{\Omega} = \Omega/\varepsilon\omega$, the nondimensionalized energy can then be written as

$$E_0(u) = \int 1/2|\mathrm{grad}\ u|^2 + 1/(2\varepsilon^2)(x^2 + \lambda_y y^2 + \lambda_z z^2)|u|^2 + 1/(4\varepsilon^4)u^4 + \boldsymbol{\Omega}\cdot(\mathrm{i}u, \mathrm{grad}\ u \times r), \tag{1}$$

where $\omega = \omega_x, \omega_y = \lambda_y\omega, \omega_z = \lambda_z\omega$, with $0 \le \lambda_y, \lambda_z \le 1$.

Due to the constraint that the integral of $|u|^2$ must be equal to 1, it is equivalent to minimizing

$$E(u) = \int |\mathrm{grad}\ u|^2 + 2\mathrm{i}[(\boldsymbol{\Omega}\times\boldsymbol{r})\cdot\mathrm{grad}\ u]u' + 1/(2\varepsilon^2)|u|^4 - 1/(\varepsilon^2)a(\boldsymbol{r})|u|^2, \tag{2}$$

*Project supported partly by the National Natural Science Foundation of China (Grant Nos 10301034 and 40574069).

†E-mail: hzh@cssar.ac.cn

where $a(\boldsymbol{r}) = \alpha - (x^2 + \lambda_y y^2 + \lambda_z z^2)$ for some constant α which is chosen so that the integral of $a(\boldsymbol{r})$ on the ellipsoid $\mathcal{D} = \{a > 0\} = \{x^2 + \lambda_y y^2 + \lambda_z z^2 < \alpha\}$ is equal to 1.

Corresponding to the physical experiments conducted recently, we may make $\boldsymbol{\Omega} = (0, 0, \Omega)^{\mathrm{T}}$; according to Refs.[3-6], the energy in Eq.(2) can be further written as $E_\varepsilon(u) = \int_{\mathcal{D}}\{|(\mathrm{grad} - \mathrm{i}A)u|^2 + 1/(2\varepsilon^2)(a_\varepsilon(\boldsymbol{r}) - |u|^2)^2 + c_\varepsilon$, where $a_\varepsilon(\boldsymbol{r}) = a(\boldsymbol{r}) + \varepsilon^2\Omega^2 r^2$, $\boldsymbol{A}$ is a vector potential defined by $\boldsymbol{A} = (y, -x, 0)^{\mathrm{T}}\Omega$, and the constant c_ε is given by $c_\varepsilon = \int_{\mathcal{D}}\{1/(2\varepsilon^2)(a^2(\boldsymbol{r}) - a_\varepsilon^2(\boldsymbol{r}))\}$.

We begin by describing the differential equations associated with the minimizers of the Gross–Pitaevskii energy as well as the time-dependent Gross–Pitaevskii equations. The minimizers of the Gross–Pitaevskii energy satisfies the equation $-(\mathrm{grad} - \mathrm{i}\ A)^2 u + 1/\varepsilon^2|u|^2 u - a_\varepsilon(\boldsymbol{r})/\varepsilon^2 u = \mu_\varepsilon(u)u$, in $\mathcal{D}$, where $\mu_\varepsilon(u)$ is a constant multiplier corresponding to the constraint $\int_{\mathcal{D}} |\phi|^2 = 1$.

To compute the minimizers of Eq.(2) numerically, we consider the time-dependent equation in the imaginary time

$$\frac{\partial u}{\partial t} = (\mathrm{grad} - \mathrm{i}\ A)^2 u - 1/\varepsilon^2|u|^2 u + a_\varepsilon(\boldsymbol{r})/\varepsilon^2 u + \mu_\varepsilon(u)u, \tag{3}$$

under the initial condition $u(\boldsymbol{r}, 0) = u_0\{\boldsymbol{r}\}$ in $\mathcal{D}$, and the boundary condition $u = 0$ on $\partial\mathcal{D}$. Here $\mu_\varepsilon(u)$ again denotes the Lagrange multiplier. If u_0 satisfies the constraint $||u_0|| = 1$, then we may determine $\mu_\varepsilon(u)$ by $\mu_\varepsilon(u) = \int_{\mathcal{D}}\{|(\mathrm{grad} - \mathrm{i}\ A)u|^2 + 1/\varepsilon^2|u|^4 - a_\varepsilon(\boldsymbol{r})/\varepsilon^2|u|^2\}\mathrm{d}\mathcal{D}$.

Discussion on the existence and uniqueness of the weak solution has been given, and the long time asymptotic behaviour may also be examined using techniques similar to those in Refs.[3–6] by Du *et al.* Some basic algorithms can be found in Refs.[12–19].

Let $\{u_n\}$ be an approximate solution of $\{u_n(t_n)\}$ at a discrete time $\{t_n\}$ with time step $\Delta t_n = t_n - t_{n-1}$. A two-step Runge–Kutta scheme is used to develop the equation in time: $u^*_{j+1} = u_j + 1/2(\Delta t)f(t_j, u_j), u_{j+1} = u_j + (\Delta t)f(t_j + 1/2\Delta t, u^*_{j+1})$, where f contains the right side of Eq.(3).

The values of constants in Eq.(3) are set to be $\varepsilon = 0.016, \lambda_y = 1, \lambda_z = 0.5$, 0.55 or 0.6; the angular frequency Ω will be varied from 14.5 to the maximum value of 28, for which no deformation of the condensate has to be taken into account.

Equation (3) is propagated in imaginary time until the evolution of the energy (2) decreases very slowly with the criterion $\mathrm{d}E/\mathrm{d}t < 10^{-3}(\mathrm{d}t = 1.0 \times 10^{-5})$ and almost reaches a local minimizer.

For the considered range of Ω, the numerical domain is fixed to an elongated box $(x, y, z) \in [-0.8, 0.8] \times [-0.8, 0.8] \times [-5.0, 5.0]$. For the following initial conditions we have computed with different meshes $100 \times 100 \times 250$ and $80 \times 80 \times 200$, and obtained the same configurations with the energy difference close to 10^{-3}, so we can conclude that a refined grid using $100 \times 100 \times 250$ nodes is appropriate, and sufficient to achieve the grid-independence for all numerical experiments considered.

In numerical simulations given in next section, we compute on the following initial conditions $u(x, y, z) = \sqrt{a(r) \cdot w(x, y, z) \cdot \exp(\mathrm{i}\theta)}$, where (r, θ) are the polar coordinates in the (x, y) plane. When $w(x, y, z) = \sqrt{x^2 + (y - 0.1 \times \tanh(1.1z))^2}$, we call it the initial condition I. When $w(x, y, z) = \sqrt{x^2 + (y - 0.1 \times \tanh(1.1z))^2}$, $z \geq 0$ and $w(x, y, z) = \sqrt{x^2 + (y + 0.1 \times \tanh(1.1z))^2}$, $z < 0$, we call it the initial condition II. Next, we choose $w(x, y, z) = \sqrt{x^2 + y^2}$ as the initial condition III, which serves to examine the effect of different initial values on vortex configurations.

3. Results and discussions

In this paper, a key point we emphasize is that $\Delta t = 10^{-5}$ only serves as the time step in numerical simulations, and as $t \to \infty$ we will have the final stable solutions, which means the energy no longer decreases. All the results reported in the following belong to this category.

In the numerical simulation, it is possible to create various S- or U-shaped vortex configurations before the solution reaches the stable state. We also

find single S- or U-shaped vortex during the imaginary time evolution; however, what we need are stable state solutions, which have the properties of some spatial or geometrical equilibrium, so that there are only four kinds of vortices as follows: i.e. vortex-free, a single completely straight vortex line superimposed on the z-axis, 3 S-shaped, 2–5 U-shaped vortices within the scope of the present paper.

3.1. Simulation results under different initial conditions

We artificially 'plant' vortices in the domain to find solutions with different shapes. As the earlier section described, under different initial conditions I and/or II, we perform some computations and obtain numerically the S-shaped or U-shaped vortices for $\Omega = 28$ and straight line for $\Omega = 24$ vortex configurations, as shown in Fig.1.

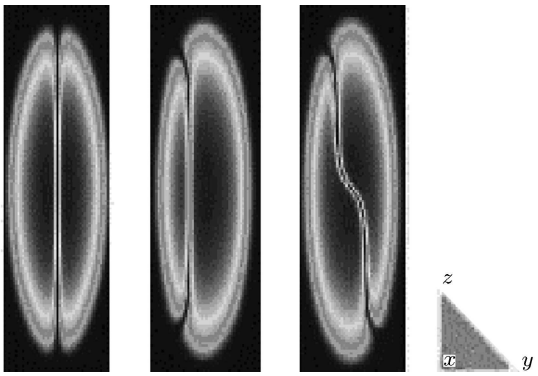


Fig.1. Stable straight-line, U- and S-shaped vortex configurations.

Here we would like to say that initial conditions are only important to simulate S- and U-shaped vortices, whereas a completely straight vortex can be observed by starting from the initial condition I or II. In the following sections, we will find that there exists transformation between S- and U-shaped vortices, indicating that angular velocity Ω has also a significant influence on vortex.

3.2. The effect of variation of Ω on the vortex number and shape

Starting the simulation with a steady state solution by increasing and decreasing the parameter Ω, we will find the solution branches with different vortex number and shape, and their transformation. First we use different initial conditions to stimulate the single or multiple vortices and obtain the different branches of solutions by varying Ω.

3.2.1. For the initial condition I

Under the initial condition I, when first starting the computation for small $\Omega(= 24)$, we only obtain a single completely straight vortex line, and we stay on this solution branch up to $\Omega = 24.581$; when the parameter Ω is increased to 24.582, three S-shaped vortex configurations are observed and they persist up to $\Omega = 28$ (see Figs.2–4).

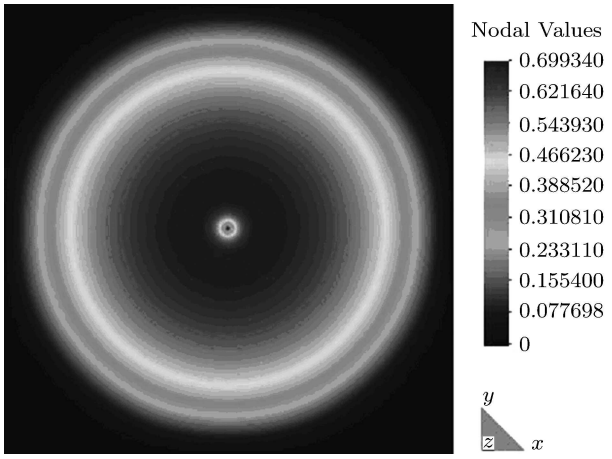


Fig.2. Straight-line vortex contour plots in the centre $z = 0$ cut plane for $\Omega = 24$.



Fig.3. 3 S-shaped vortex iso-surface picture taken from different angles.

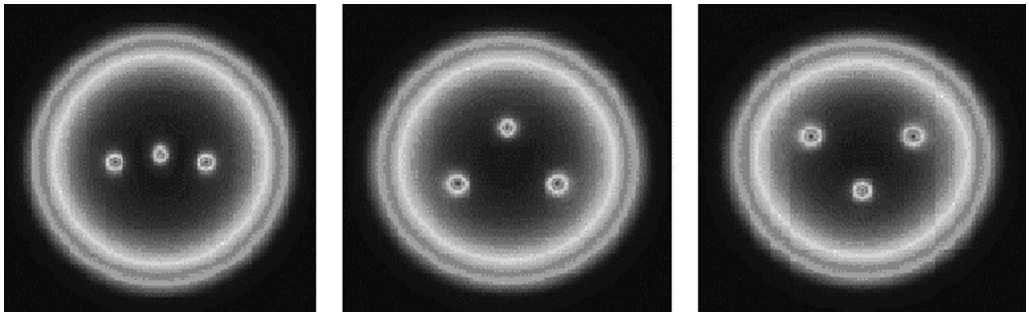


Fig.4. 3 S-shaped vortex contour plots with cut planes z =0, 1, and −1 for $\Omega = 25$.

3.2.2. For the initial condition II

Under the initial condition II, when we employ the numerical experiments similar to the above, at first no vortex emerges at $\Omega = 24.5$; next at larger $\Omega = 24.66$, again the single straight vortex appears, and then 3 U-shaped vortices appear when Ω is varied from 24.665 to 28, as shown in Fig.5.

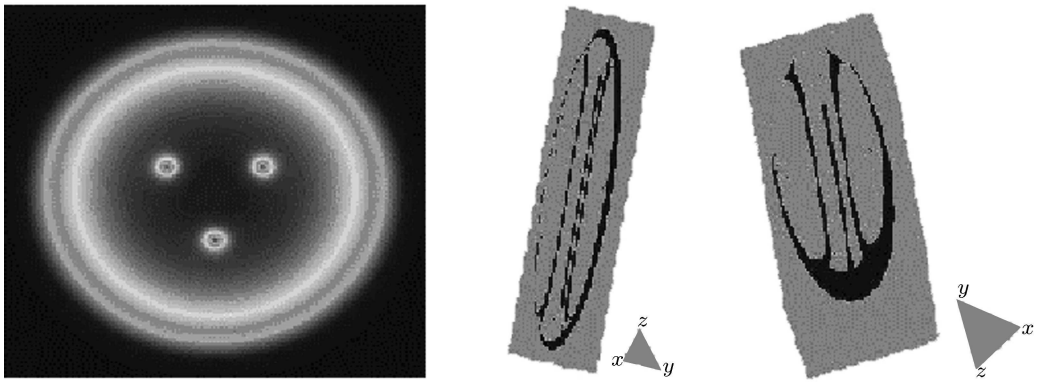


Fig.5. 3 U-shaped vortex configurations for $\Omega = 24.7$.

3.2.3. For a steady state solution with vortices

The authors of Ref.[3] also mentioned another strategy for obtaining multiple-vortex configurations, that is, to start the computation from a vortex-free steady state, and then to abruptly increase Ω to a very high value. Here we apply the opposite strategy for Ω, i.e., decreasing Ω to a small value 14.5, when choosing the stable state solution of the 3 U-shaped vortices in the above subsection as the initial condition. Figure 6 shows that 3 U-shaped vortices can exist down to $\Omega =$ 14.5 when only two U-shaped vortices retain. Under the initial condition III, we find that 3 U-shaped vortex configurations are obtained for $\Omega = 25$, and with the same experiments: the 3-vortex branch switches to 2 U-shaped vortices when Ω is decreased down to 14.

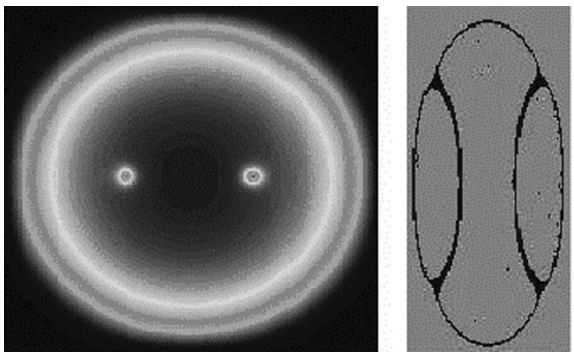


Fig.6. 2 U-shaped vortices for $\Omega = 14.5$.

3.3. The transformation between S-shaped and U-shaped vortices

The variation of Ω has often been used to follow a particular solution branch. The variation procedure also provides a test for the local stability of the nu-

merical solutions: when one branch becomes unstable, the solution jumps onto a different branch.[3] Starting from the 3 S-shaped vortices, from which it is interesting to observe the transformation to 3 U-shaped ones if Ω is decreased a little. We think it is because the difference in energy and angular momentum between U and S vortices is very small, and S vortex is almost like a U one with a half-part rotated by 180 degrees.

Figure 7 gives a complete vortex transformation process from S- to U-shaped vortex. From the stable 3 S-shaped vortices whose energy is -1021.46, by decreasing Ω step by step to 24, 23, 21, 19, and 17, we obtain their energy values of -981.4, -945.9, -886.0, -837.1, -795.9 respectively. According to Table 1, it is easy to see that we will obtain the corresponding-shaped vortices when the energy value approaches a definite value for S- or U-shaped vortex.

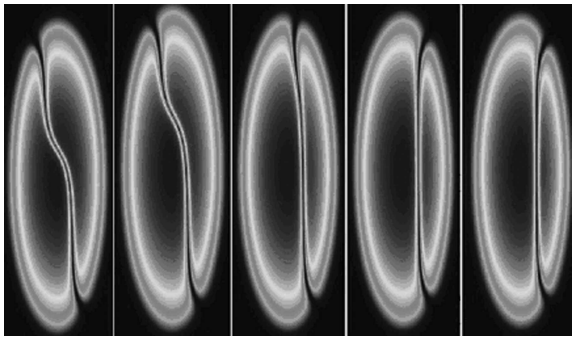


Fig.7. The transformation of vortices from S- to U-shaped.

Table 1. Energy values for the different initial conditions.

Ω	17	18	19	20	21	22	23	24	25
Cond I	-797.1	-814.8	-835.8	-859.3	-885.3	-914.1	-945.9	-981.4	-1021.5
Cond II	-795.6	-815.5	-837.2	-861.1	-887.2	-915.9	-947.7	-983.1	-1023.1
Cond III	-795.6	-815.5	-837.2	-861.1	-887.2	-915.9	-947.7	-983.1	-1023.1

3.4. The effect of the dimensions of ellipsoid on the number and shape of the vortex

We introduce a new technique to obtain multiple vortices by increasing λ_z to a certain level while keeping Ω unchanged.

We recall only a vortex-free solution for $\Omega = 24.5$ starting from the initial condition I. If λ_z varies from 0.5 to 0.55, 4 U-shape vortices are obtained as shown in Fig.8. Similarly, when we use the initial condition II, we have a straight vortex line for $\Omega = 24$; when increasing λ_z from 0.5 to 0.6, we will have 5 U-shape vortex configurations.

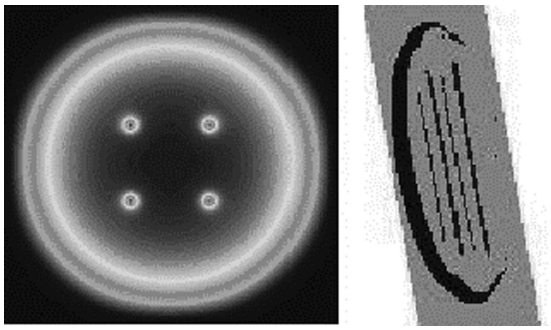


Fig.8. 4 U-shaped vortex configurations for $\lambda_z = 0.55$.

3.5. Energy diagrams

In the previous subsections, we only present some typical examples with various vortex configurations and their evolution when Ω varies. Here we give a complete energy diagram in order to have an overall view of 'the whole life of vortex from its birth to death'.

We have plotted the energies obtained under the different initial conditions, from which subtracted their energies of the basic vortex solution, as a function of Ω in Fig.9.

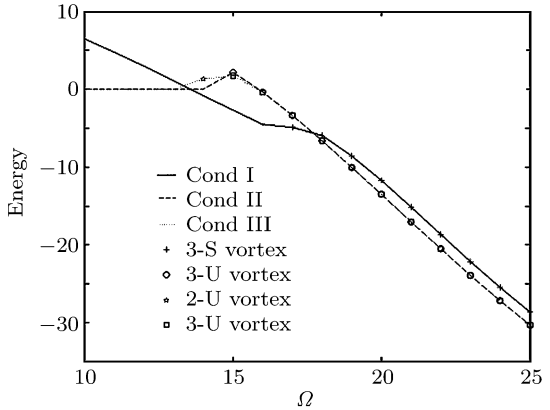


Fig.9. The energies obtained under the different initial conditions, from which subtracted their energies of the vortex-free solution, as a function of Ω.

The single-vortex solution is obtained under the initial condition I. We find that 3 S-shaped vortices will emerge when the energy difference decreases ($\Omega \geq 17$). Under the initial condition II by which we obtain vortex-free solution for $\Omega = 14$, we can have 2 U-shaped vortices and 3 U-shaped ones for $\Omega = 15$ to 25; 3 U-shaped vortices are generated when $\Omega \geq 15$ under the initial condition III.

4. Conclusion

By studying the numerical solution of Gross–Pitaevskii equations in the framework of ENS experiment, we have carried out 3D numerical simulations and obtained some results for rotating Bose–Einstein condensates in 3 dimensions. We have obtained straight line, various S- and U-shaped vortices and multiple-vortex configurations. Parallel processing of 3D Gross–Pitaevskii problem is necessary and efficient, which makes the computation based on recent physical experiments about the 3D structures of vortices faster.

Acknowledgment

The authors thank Professor Du Q very much for his important discussions.

References

[1] Rosenbuch P, Bretin V and Dalibard J 2002 *Phys. Rev. Lett.* **89** 200403
[2] Svidzinsky A A and Fetter A L 2000 *Phys. Rev. Lett.* **84** 5919
[3] Aftalion A and Danaila I 2003 cond-mat/0303416, 0309668
[4] Aftalion A and Du Q 2001 cond-mat/0103299
[5] Du Q *Recent Progress in Computational and Applied PDEs* (New York: Kluwer/Plenum)
[6] Du Q, Gunzburger M D and Peterson J S 1992 *Phys. Rev.* B **46** 9027
[7] Kengne E and Liu W M 2006 *Phys. Rev.* E **73** 026603
[8] Liu W M, Fan W B, Zheng W M, Liang J Q and Chui S T 2002 *Phys. Rev. Lett.* **88** 170408
[9] Liu W M, Wu B and Niu Q 2000 *Phys. Rev. Lett.* **84** 2294
[10] Lu J 2004 *Chin. Phys.* **13** 811
[11] Xu Y, Jia D J, Li X J, Zuo W and Li F S 2004 *Acta Phys. Sin.* **53** 2831 (in Chinese)
[12] Du Q, Huang Z H and Wang D S 2005 *Numer. Meth. Part. Differ. Equ.* **21** 8592
[13] Huang Z H, Lei G Y and Liu X P 2000 *Chin. Comput. Phys.* **21** 401
[14] Huang Z H and Chang Q S 2003 *Acta Math. Appl. Sin.* **26** 443
[15] Huang Z H and Chang Q S 2001 *Chin. Comput. Phys.* **18** 423
[16] Huang Z H and Chang Q S 2003 *J. Comput. Math.* **21** 421
[17] Huang Z H and Shi P L 2007 *Appl. Math. Lett.* **d**oi 10.1016/j. aml. 2006. 05. 002
[18] Lei G Y and Huang Z H 1999 *Chin. J. Comput. Phys.* **16** 279
[19] Lei G Y and Huang Z H 1996 *Chin. J. Comput. Phys.* **13** 489